The photochemical ring-opening reaction of 1,3-cyclohexadiene: identifying the true reactive state

Oksana Travnikova[1,‡], Tomislav Piteša[2,‡], Aurora Ponzi[2], Marin Sapunar[2], Richard J. Squibb[3], Robert Richter[4], Paola Finetti[4], Michele Di Fraia[4], Alberto De Fanis[5], Nicola Mahne[6], Michele Manfredda[4], Vitali Zhaunerchyk[3], Tatiana Marchenko[1], Renaud Guillemin[1], Loic Journel[1], Kevin C. Prince[4], Carlo Callegari[4], Marc Simon[1], Raimund Feifel[3], Piero Decleva[7], Nađa Došlić[2,*] and Maria Novella Piancastelli[1,8,*]

[1]Sorbonne Université, CNRS, Laboratoire de Chimie Physique-Matière et Rayonnement, LCPMR, F-75005, Paris, France
[2]Institut Ruđer Bošković, HR-10000 Zagreb, Croatia
[3]Department of Physics, University of Gothenburg, SE-412 96 Gothenburg, Sweden
[4]Elettra-Sincrotrone Trieste, 34149 Basovizza, Trieste, Italy
[5]European XFEL, D-22869 Schenefeld, Germany
[6]IOM-CNR, S.S. 14 km 163.5 in Area Science Park, 34149 Trieste, Italy
[7]Dipartimento di Scienze Chimiche e Farmaceutiche, Universitá di Trieste, I-34127 Trieste, Italy
[8]Department of Physics and Astronomy, Uppsala University, SE-751 20 Uppsala, Sweden

KEYWORDS. 1,3-cyclohexadiene, photoinduced ring opening, time-resolved photoelectron spectroscopy, diabatization.

ABSTRACT: The photochemically induced ring-opening isomerization reaction of 1,3-cyclohexadiene (CHD) to 1,3,5-hexatriene (HT) is a textbook example of a pericyclic reaction, and has been amply investigated with advanced spectroscopic techniques. The main open question has been the identification of the single reactive state which drives the process. The generally accepted description of the isomerization pathway starts with a valence excitation to the lowest-lying bright state, followed by a passage through a conical intersection to the lowest-lying doubly excited state, and finally a branching between either the return to the ground state of the cyclic molecule or the actual ring-opening reaction leading to the open-chain isomer. Here in a joint experimental and computational effort we demonstrate that the evolution of the excitation-deexcitation process is much more complex than usually described. In particular, we show that an initially high-lying electronic state smoothly decreasing in energy along the reaction path plays a key role in the ring-opening reaction.

INTRODUCTION

The photochemical ring-opening reaction of 1,3-cyclohexadiene (CHD) to 1,3,5-hexatriene (HT) is a textbook example of a pericyclic reaction.[1,2] In addition to many theoretical investigations,[3–12] the dynamical evolution of photoexcited CHD has been studied, possibly more than any other photochemical reaction, with a large variety of spectroscopic techniques for isolated-molecules, i.e. in collision-free conditions and without solvent effects (see e.g. [13–21]). This pronounced interest arises from the fundamental importance of the reaction, its biological relevance[22,23] and a range of applications in organic synthesis and materials science.[24–28]

The conceptual framework to understand the photochemistry of CHD is provided by the Woodward–Hoffmann rules,[29] extended by van der Lugt and Oosterhoff[30,31] and stating that the conrotatory ring opening reaction is mediated by a doubly-excited electronic state of the same symmetry as the ground state (1^1A^-). In the ring-opening reaction, the LUMO orbital of CHD, which is doubly occupied in the reactive state, becomes the HOMO of HT. The generally accepted sequence of events starts with a valence excitation by a wavelength of about 267 nm to the first (S_1) bright state, labelled 1^1B, followed by a passage through a conical intersection (CoIn) to a dark state, labelled 2^1A^-. The following step is a branching between two pathways at a second CoIn, either the return to the ground state of the cyclic molecule or the actual ring-opening reaction leading to the open-chain isomer

(see e.g. [11–14]). Notice that the labels above and throughout the text indicate diabatic states and that we use the notation for alternant π-systems (*plus* and *minus)* pseudo-symmetry.[32,33]

In general, photochemical reactions are assumed to be driven by conical intersections (CoIns) at which two adiabatic Born–Oppenheimer potential energy surfaces (PESs) become degenerate and which act as effective funnels for transfer of population between different adiabatic PESs.[34-36] In contrast to adiabatic PESs, which suddenly change their chemical character near a CoIn, PESs that retain their character and cross at CoIns are known as diabatic states. Since properties such as the electronic transition dipole moment change smoothly only in the diabatic representation, the dynamics of the diabatic electronic populations is the one monitored in time-resolved ultrafast spectroscopy.[37]

Despite tremendous efforts, a conclusive proof of the reactivity of the diabatic 2^1A^- state has not yet been achieved. To address this problem, we ask a seemingly simple question: is there any other electronic state of symmetry A and partial double excitation character that may be involved in the ring-opening reaction in CHD? Here in a joint experimental and computational effort we show that the evolution of the process is more complex than usually described. In particular, we show that a high-lying state with a pronounced double-excitation character, labeled 3^1A^-, plays a key role in the ring-opening reaction.

To observe the first stages of a photochemical process, a suitable method is to prepare a photoexcited state with an optical laser, the so-called pump, and then follow its evolution by valence photoelectron spectroscopy, the so-called probe, as a function of pump-probe time delay with resolution on the picosecond (ps, 10^{-12} s) or femtosecond (fs, 10^{-15} s) time scale. Time-resolved photoemission is the first-choice technique to follow the evolution of a system since it provides information on both electronic and nuclear dynamics. Furthermore, it provides information on states which are not reachable by absorption methods, in particular dark states which need to be characterized in the present case.

A breakthrough in this direction is represented by the FERMI free-electron laser (FEL) at the Elettra facility, Trieste, Italy. Time-resolved photoemission spectra can be obtained there with spectral resolution high enough to precisely characterize ionization from electronic states even if they are weak and/or close in energy (see e.g. [38,39]). FERMI as a seeded FEL offers the advantages of a narrow photon energy bandwidth, negligible photon energy jitter, and higher stability, higher pulse energies and much higher photon fluxes with respect to monochromatized sources based on high harmonics generation (HHG).

RESULTS AND DISCUSSION

Our experiments were performed at FERMI on the beam line LDM, devoted to atomic and molecular spectroscopy studies.[40] The pump was a titanium-sapphire optical laser, providing a wavelength of 267 nm, and the probe was valence photoelectron spectroscopy with a photon energy of 19.23 eV. The delay time range was from -1 to 2 ps, spanned in steps of 50-100 fs. We recorded valence photoelectron spectra with a magnetic bottle spectrometer[41,42] (see Supporting Information, SI, for further details on the facility, the beam line and the spectrometer).

In Figure 1, upper panels (experiment and theory) we show valence photoelectron spectra recorded for several values of pump-probe delay in the delay range from -1 to 2 ps in steps of 100 fs. The spectra are plotted as a two-dimensional map, highlighting the variations in spectral intensity as a function of time delay. The ground-state spectrum is subtracted from the spectra obtained at later times (see SI and Figs. S2-S4 for further details on how the experimental spectra are obtained). The upper panels illustrate the variation of the photoionization signal as a function of the pump-probe delay, the changes of averaged signals in the four characteristic areas are shown in the lower panels (experiment and theory). We notice the development of a series of new features in two electron energy regions, i.e. at low binding energy (4-8 eV) and around 10 eV. The low-binding-energy region is characteristic of spectral features related to excited states or dynamic features due to the photoexcitation process, while the 10 eV region is in the range characteristic of ground-state features.

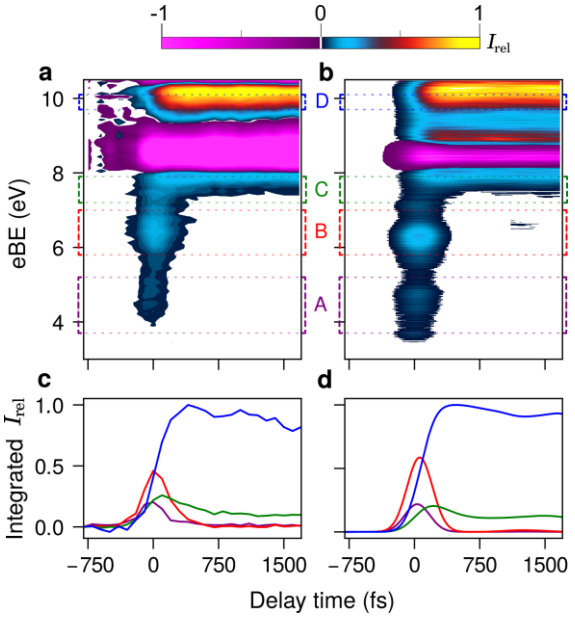

Figure 1. **a)** Experimental and **b)** computed differential 2D maps of photoelectron spectra of CHD. White color denotes the regions with $|I_{rel}| < 0.01$. For computed excited-state-absorption (ESA) component of the signal (separated on CHD- and HT-ending trajectories), check Fig. S5. **c)** Experimental and **d)** computed time evolution of the spectral intensity integrated over the area marked by colored rectangles in **a).** For experimental and computational details, see the SI.

The three features in the low-binding-energy region have a different behavior as a function of delay: the two peaks at 4.5 and 6.4 eV binding energy reach maxima at 0 ps

and decrease to zero intensity after 0.5 ps, while the third feature at 7.5 eV has low intensity at 0 ps, continues to grow to a maximum at 0.5 ps and finally stabilizes after about 1 ps. The feature at high binding energy, 9.9 eV, grows after 0 ps as a function of delay, and stays constant after about 0.5 ps. We denote these features A, B, C and D in order of increasing binding energy. The disappearing features A and B are "feeding" the developing ones C and D, giving evidence of a dynamical change accompanying the electronic relaxation. This is a first hint that features A and B correspond to excited states which relax on a fs time scale, while the features C and D developing and then reaching an asymptotic value are connected to electronic states belonging to vibrationally hot open chain and/or closed ring isomers.

This assignment is strongly supported by theory. The photoinduced dynamics was simulated with non-adiabatic surface-hopping trajectories. In this method an ensamble of classical trajectories is propagated starting in the excited state and the stochastic fewest switches algorithm REF[Tully] is used to allow each trajectory to "hop" to a different electronic state. The "hops" are governed by the non-adiabatic couplings between electronic states. In this work, a total of 107 trajectories were propagated for 2000 fs with a time step of 0.5 fs in a manifold of first three singlet electronic states (S0, S1 and S2). The energies and forces needed for propagation of the trajectories are computed using the XMS(3)-CASPT2(6,6) method, whose accuracy was assessed in Ref. 12. (see the Computational section and SI for details). The photoelectron spectra were computed in the sudden approximation in which the partial cross sections are approximated with Dyson orbital norms. The accuracy of the sudden approximation was assessed by comparison with the benchmark spectrum computed using a B-spline description of the photoelectron continuum (see Figure S6). To match the experiment, the theoretical spectra have been shifted by +0.3 eV. For further details on how the theoretical spectra are calculated see the Methods section and SI. The agreement between the experimental and simulated spectra is remarkably good, both in terms of intensity and time evolution of the peaks, with the width of the ground-state bleach component (purple) being the only major discrepancy. The simulated spectra, when analyzed separately for non-reactive (CHD) and reactive (HT) trajectories (see Fig. S5) show that band C arises mainly from vibrationally hot CHD, while the band D is dominantly due to newly formed HT molecules. The latter assignment is confirmed by a comparison between the ground-state valence photoelectron spectra of CHD and HT, where there is spectral intensity in the binding energy region around 10 eV only for the open-chain isomer.[43,44]

While the assignment of features C and D is rather straightforward, the behaviour of features A and B, which correspond to excited states and therefore are the key to identify the true reactive one, is more complex. A first hint of the three-state model reported in the literature being oversimplified is that we do not observe a simple series of few peaks growing and decreasing in temporal sequence, as e.g. was reported in Ref.[38] for acetylacetone, where the adiabatic description was sufficient.

To fully explain the mechanism of the reaction, we need to connect the evolution of the photoionization bands as a function of time with the population of the diabatic electronic states involved in the reaction. To this end we first consider the properties of the electronic states at the Franck-Condon geometry. The electronic spectrum of CHD reported in the literature is composed of two broad bands at ~5.0 and ~8.0 eV.[45] The first encompasses the bright $1^1A^- \rightarrow 1^1B$ and dark $1^1A^- \rightarrow 2^1A^-$ transitions. The second or *cis*-band is characteristic for *cis*-polyenes. Here two valence transitions of mixed character have been identified – the intense $1^1A^- \rightarrow 1^1A^+$ transition at 8.0 eV[4,46] and a higher-lying transition with considerable vibronic structure.[45] Intercalated between these two bands are several sharp Rydberg transitions.[4,46,47] Owing to their weak coordinate dependence, Rydberg states are expected to play a negligible role in the ring-opening reaction.

Vertical excitation energies of the six lowest valence excited states of CHD with the coefficients of the leading configuration state functions (CSFs) are collected in Table 1 (for EOM-CC3 results see Table S1), while the orbitals constituting the active space are illustrated in Fig. S7.

Table 1. State ordering and vertical excitation energies (in eV) of the six lowest valence-excited states at the Franck-Condon geometry labeled according to *plus-minus* alternancy symmetry, leading configurational state functions (CSFs) and their CI coefficients calculated at the XMS(7)-CASPT2[6e,6o] level of theory. For EOM-CC3 states, see Table S1.

State	E / eV (f)	Exp.[a] E / eV	Leading CSFs	CI coeff.
1^1A^-	-	-	Aufbau	0.96
			$\pi_2\pi_2 \rightarrow \pi_1^*\pi_1^*$	−0.14
1^1B	5.18 (0.017)	4.94	$\pi_2 \rightarrow \pi_1^*$	0.97
2^1A^-	5.99 (0.008)	-	$\pi_2\pi_2 \rightarrow \pi_1^*\pi_1^*$	0.53
			$\pi_1 \rightarrow \pi_1^*$	−0.55
			$\pi_2 \rightarrow \pi_2^*$	0.46
2^1B	7.50 (0.007)	-	$\sigma \rightarrow \pi_1^*$	0.97
1^1A^+	8.31 (0.321)	7.90	$\pi_1 \rightarrow \pi_1^*$	0.69
			$\pi_2 \rightarrow \pi_2^*$	0.65
			$\pi_2\pi_2 \rightarrow \pi_1^*\pi_1^*$	0.16
3^1A^-	8.66 (0.217)	-	$\pi_2\pi_2 \rightarrow \pi_1^*\pi_1^*$	0.68
			$\pi_2 \rightarrow \pi_2^*$	−0.51

			$\pi_1 \rightarrow \pi_1^*$	0.28
3^1B	10.11 (0.000)	-	$\pi_1 \rightarrow \pi_2^*$	0.96
[a]Optical and electron energy loss spectroscopies[48].				

The main results are summarized in Figure 2. At the Franck-Condon geometry, the XMS(7)-CASPT2[6e,6o] method yields the 1^1B state at 5.18 eV, the dark 2^1A^- state at 5.99 eV and the two bright states of the *cis*-band, 1^1A^+ and 3^1A^-, at 8.31 and 8.66 eV, respectively. The electron density differences between the excited states and the ground state plotted in Fig. 2a show that excitation to the 1^1B and 3^1A^- states leads to depletion of electron density on the C_1-C_6 bond, while excitation to 2^1A^- and 1^1A^+ leaves the density on that bond nearly unchanged. From the wave functions of the three states of symmetry A, which are dominated by the three CSFs shown in Fig. 2b, it is evident that the 3^1A^- state has a pronounced double-excitation character (see CI coefficients) and the overall electronic properties of a potentially reactive state.

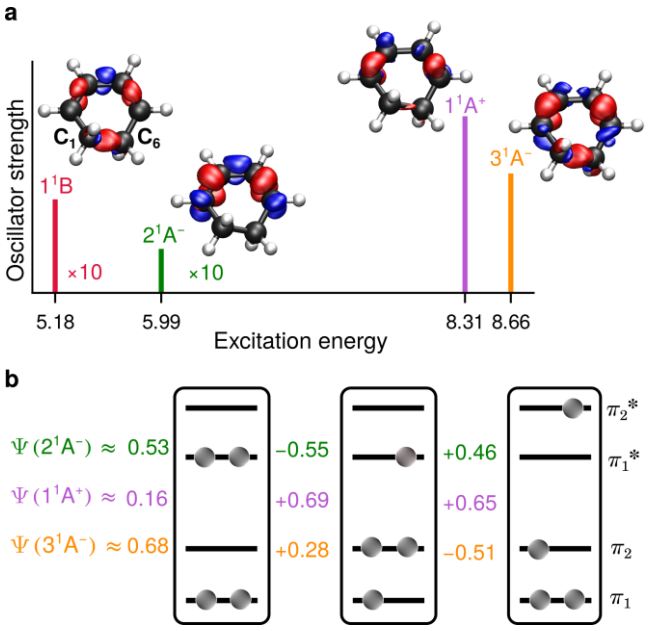

Figure 2. **a)** Excitation energies and relative absorption intensities of the 1^1B, 2^1A^-, 1^1A^+ and 3^1A^- states (sticks) and the corresponding maps showing the electron density difference with respect to the electronic ground state calculated at the Franck-Condon geometry. Areas of increased and reduced electron density are shown in blue and red, respectively. **b)** The three valence states, 2^1A^- (green), 1^1A^+ (purple) and 3^1A^- (orange), with the CI coefficients of the three dominant CSFs ($\pi_2\pi_2 \rightarrow \pi_1^*\pi_1^*$, $\pi_1 \rightarrow \pi_1^*$ and $\pi_2 \rightarrow \pi_2^*$).

Figure 3 shows the one-dimensional potential energy profiles of the adiabatic (black) and diabatic (colours) states along the ring-opening path in C_2 symmetry. The diabatization has been performed in the basis of the lowest six adiabatic states by minimizing the variation of their wave functions along the reaction path.[49] The diabatization in the usual basis of the three lowest diabatic states, as defined at the FC geometry, is shown in Figures S8 (see also S9). Details of the procedure are given in the SI. One sees that the coordinate dependence of the diabatic 1^1B state (red) matches the expected behavior, but this is not the case for the 2^1A^- state (green), which clearly increases in energy (destabilizes) along the reaction path. The diabatic 3^1A^- state (orange) is the state that is strongly stabilized in the reaction. The two states cross at $R(C_1\text{-}C_6)$ ~1.9 Å where the adiabatic S_2 state shows the characteristic inflection. Further down the reaction path, 3^1A^- crosses with the 1^1B state and at $R(C_1\text{-}C_6)$ ~ 2.3 Å with the ground state. This indicates that the ground state of HT correlates with the 3^1A^- state and not with the 2^1A^- state. Notice that the proposed pathway does not contradict the Woodward-Hoffmann rules as they do not prescribe that the reaction should proceed on the *lowest* doubly excited state at the FC geometry.

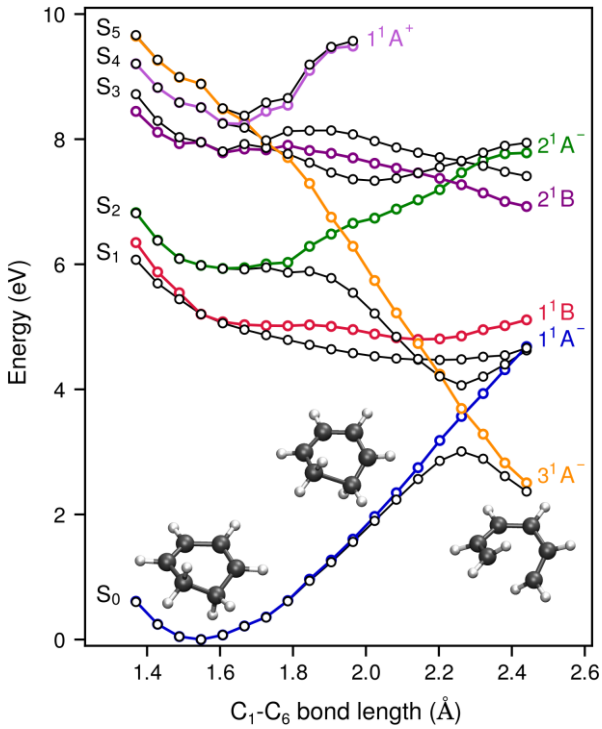

Figure 3. Coordinate dependence of the potential energy of the lowest adiabatic electronic states (black) and diabatic electronic states: 1^1A^- (blue), 1^1B (red), 2^1A^- (green), 2^1B (dark violet), 1^1A^+ (light violet) and 3^1A^- (orange). For comparison with the traditional three-state model see the Fig. S8.

To understand the role of the different diabatic states in the ring-opening reaction when the C_2 symmetry is lifted, we analyse two representative non-adiabatic trajectories yielding CHD (Fig. 4a-4c) and HT (Fig. 4d-4f). For additional trajectories see Fig. S10. The two trajectories exhibit a very similar behaviour up to the CoIn with the ground state. In both cases the dynamics is initiated in the S_1 state (Fig 4a and 4d), which is in the diabatic 1^1B state (Fig. 4b and 4e). At two instances, at ~10 and ~25 fs, the gap between the S_1 and S_2 states becomes vanishingly small and the S_1 state has a possibility to change its character. In-

deed, the diabatic populations show a brief increase of the 2^1A^- contribution at ~10 fs (green), but then the 1^1B character is recovered until ~25 fs when its contribution suddenly drops. From ~25 fs onward the S_1 state is best described as a superposition of the 1^1A^- (blue) and 3^1A^- (orange) diabatic states. The two states are strongly coupled by nuclear motion along the so-called extended bond alternation coordinate (BAC*), which is the difference of single and double bonds lengths in HT plus $R(C_1\text{-}C_6)$.[11] In the CHD trajectory the return to the ground state occurs after a BAC* local maximum, while the $C_1\text{-}C_6$ bond is compressing and the S_1 state is dominantly of 1^1A^- character. On the contrary, in the HT trajectory the CoIn with the ground state is encountered after a BAC* local minimum, while the $C_1\text{-}C_6$ bond is expanding and the S_1 state is dominantly of 3^1A^- character. After the hop the CHT trajectory continues to evolve in the 1^1A^- state and the HT trajectory in the 3^1A^- state, which is now the ground state leading to the HT product. Altogether, our analysis suggests that the fate of a nonadiabatic trajectory is determined by the character of the S_1 state at the moment of the $S_1 \rightarrow S_0$ nonadiabatic transition. If the transition occurs when the S_1 state has a dominant 1^1A^- character, the CHD product is formed and, *vice versa*, if the hop occurs when the S_1 state has a dominant 3^1A^- character the HT product is formed.The analysis of the ensemble of non-adiabatic trajectories, divided in two groups, CHD and HT, and synchronized in such a way as to reach the S_1/S_0 CoIn at the same time, is given in Figures 4g-4h. Fig. 4g shows that for all HT trajectories the BAC* is increasing before the hop to S_0, while it is decreasing for most but not all CHD trajectories. The distribution of $R(C_1\text{-}C_6)$ and BAC* at the time of hop (Fig. 4h) indicates that for large BAC* and $R(C_1\text{-}C_6)$ distances both CHD (blue) and HT (orange) can be formed in a close to 50:50 ratio but for small BAC* and short $R(C_1\text{-}C_6)$ only CHD is formed, irrespectively of whether BAC* is compressing or not. A closer inspection reveals that in this group of non-reactive trajectories the population of the 3^1A^- state is negligibly small (see Fig. S11), meaning that the existence of a second non-reactive pathway from either 1^1B or 2^1A^- cannot be excluded.We can now relate the average adiabatic and diabatic electronic populations to the time evolution of the two lowest-energy bands in the photoelectron spectra. Figure 5a shows the two-dimensional map of unconvoluted theoretical photoelectron spectra at short delay times. Two bands are clearly visible in the binding energy range of 3-7 eV. Band A starts at ~3.2 eV and within 15 fs reaches a plateau at ~4.5. eV. It arises from the $S_1 \rightarrow D_0$ transition.

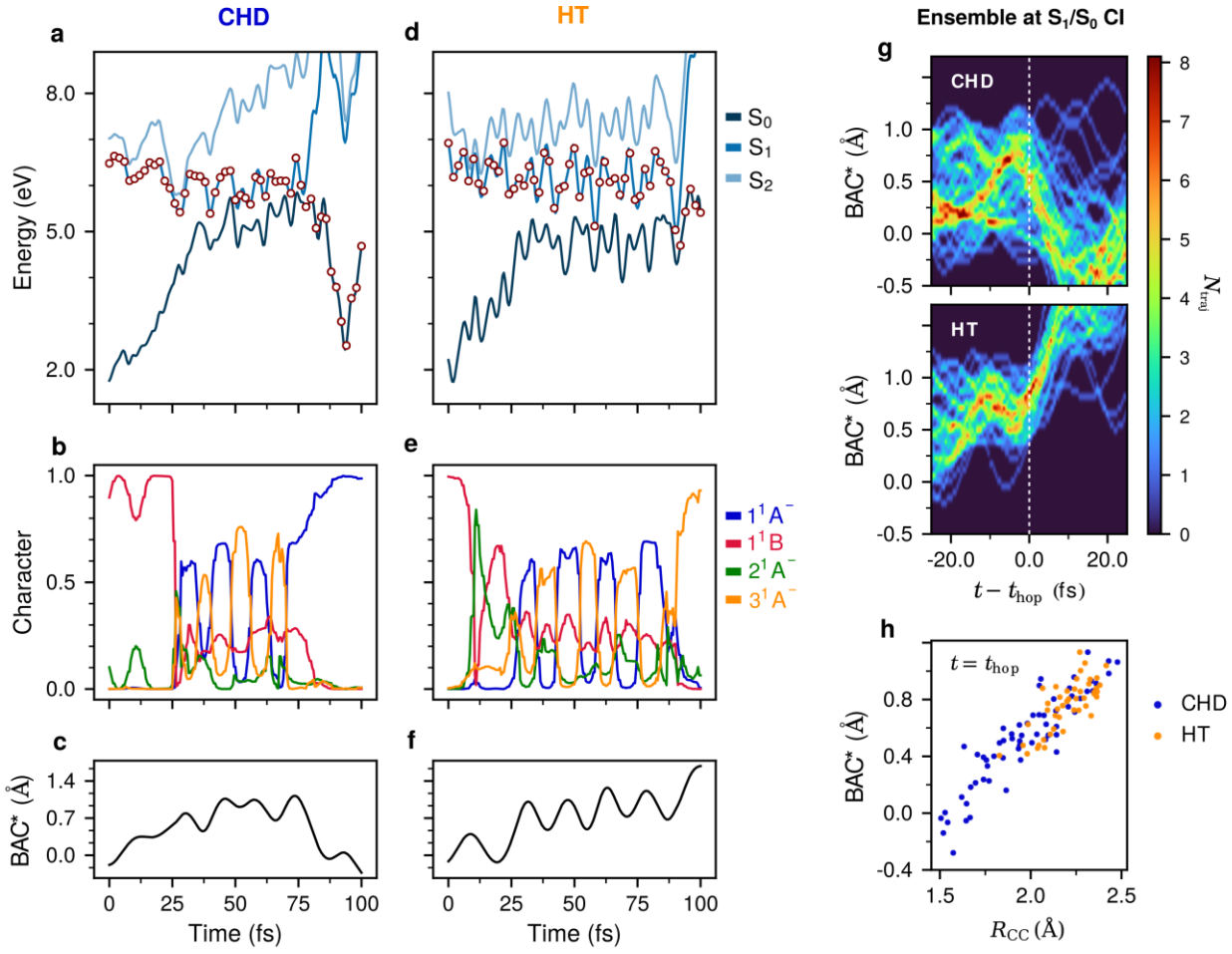

Figure 4. Two representative nonadiabatic trajectories leading to CHD (**a**-**c**) and HT (**d**-**f**). **a**) and **d**) Time evolution of the potential energy of the electronic ground state S_0 (dark blue) and the two lowest excited states S_1 (blue) and S_2 (light blue). Dots mark the instantaneous populations of electronic states. **b**) and **e**) Decomposition of the currently populated state in terms of four diabatic states, 1^1A^- (blue), 1^1B (red), 2^1A^- (green) and 3^1A^- (orange) along the trajectories. **c**) and **f**) Time evolution of the extended bond alternation coordinate (BAC*) along the nonadiabatic trajectories. **g**) Evolution of the BAC* coordinate for the ensemble of nonadiabatic trajectories synchronised to reach the S_1/S_0 CoIn simultaneously at $t' = t - t_{hop} = 0$. At the moment of hop BAC* is decreasing for CHD and increasing for HT trajectories. For the evolution of the $R(C_1\text{-}C_6)$ coordinate and relative velocity, $dR(C_1\text{-}C_6)/dt$, see Figure S13. **h**) Distribution of $R(C_1\text{-}C_6)$ and BAC* at the moment of hop to S_0. Orange (blue) circles correspond to HT (CHD) trajectories. For other structural parameters see Fig. S14.

The increase of the ionization energy is caused by the motion toward the minimum of the S_1 state. As this motion leads to the extension of the $C_1\text{-}C_6$ bond, the energy of the ground state of the CHD cation (D_0) increases (see Fig. S12). At around ~30 fs the band loses intensity. Band B starts at ~7.0 eV but it is almost immediately stabilized to the 5.8-6.2 eV binding energy range. The sudden stabilization of band B is caused by the crossing of the cationic D_1 and D_2 states (see Fig. S9). The maximum of the intensity of band B is reached at ~40 fs. Fig. 5b shows the average population of the adiabatic states S_0, S_1 and S_2 as obtained from nonadiabatic dynamics simulations. By comparing the time evolution of bands A and B with the average population of the adiabatic states one sees that the loss of intensity of band A coincides with the transfer of population from the S_1 to the S_2 state with maximum at ~30 fs, while the maximum of the intensity of band B at ~40 fs coincides with the rather counterintuitive rise of the population of the S_0 state. The electronic populations of the diabatic states (Fig. 5c) provide a more consistent view. The population initially residing in the 1^1B state steadily decreases. The 2^1A^- state is transiently populated at early times but its population never exceeds 0.2. In the ~35-55 fs interval the population of the 1^1A^- (blue) and 3^1A^- (orange) states increases and the system evolves in a superposition of these two states. This interval coincides with the maximum of the intensity of band B. The decomposition of the photoelectron spectra into contributions from diabatic states in Figs. 5d-5g unambiguously shows that the increase of the intensity of band B at around 40 fs originates from the population of the 3^1A^- state (Fig. 5g). As the reaction proceeds, the formation of

the CHD and HT product correlating with the 1^1A^- and 3^1A^- states, respectively, becomes clearly visible.

Our analysis clearly points towards a predominant role of the 3^1A^- diabatic state in the reactive path, and in general that a more consistent picture of the overall dynamics can be achieved by analyzing diabatic rather than adiabatic contributions. We consider these findings as a step forward with respect to the description usually reported in the literature.[11–21] We rely on both experimental advances, such as the possibility of measuring time-resolved valence photoelectron spectra with rather high electron energy resolution, and theoretical methods allowing accurate calculation of the photoelectron signal and on-the-fly adiabatic-to-diabatic transformation of electronic populations.

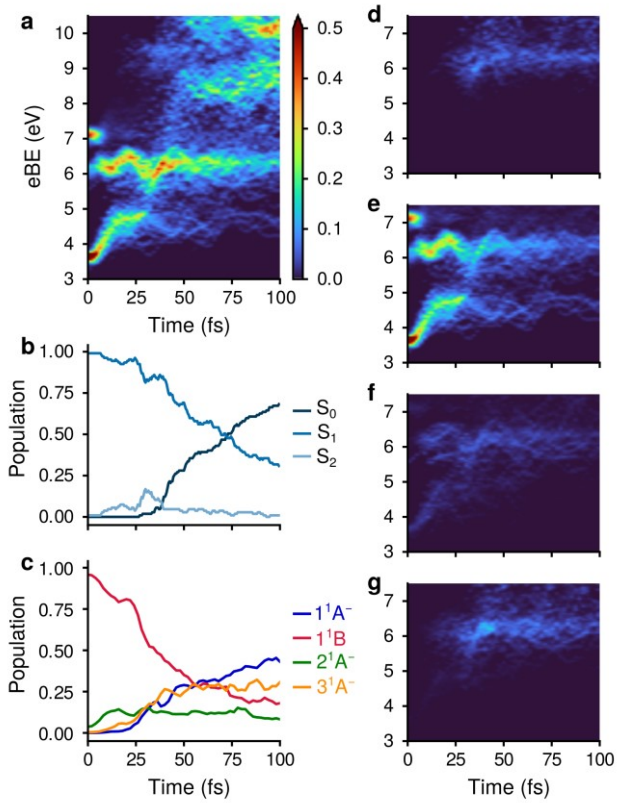

Figure 5. **a)** Unconvoluted photoelectron spectra for short delay times. The ground state bleach component is not taken into account. **b)** Time evolution of the adiabatic population of electronic states obtained from surface hopping nonadiabatic dynamics simulations. **c)** Time evolution of the diabatic population of electronic states obtained by diabatization of electronic states along nonadiabatic trajectories. **d)**-**g)** Decomposition of the photoionization spectrum in terms of contributions of the diabatic states 1^1A^- (**d**), 1^1B (**e**), 2^1A^- (**f**), 3^1A^- (**g**).

CONCLUSION

The photochemical ring-opening reaction of 1,3-cyclohexadiene (CHD) to 1,3,5-hexatriene (HT) is a textbook example of a pericyclic reaction, and possibly the most investigated isomerization reaction with advanced time-resolved spectroscopies. Here we provide a new insight into the mechanism of the reaction. In particular, we show that the doubly excited dark state, labeled 2^1A^-, which is considered in the literature the gateway to the isomerization process, does not play a significant role. Instead, an initially high-lying state, labeled 3^1A^-, with a pronounced double excitation character and a significant reduction of electron density upon the C_1-C_6 bond (the one which breaks during the isomerization process), is the reactive state whose temporal evolution drives the reaction.

METHODS

Experimental. The experiments were performed at the low-density matter (LDM) beamline[40] at the FERMI free-electron laser facility. The Ti:Sapphire optical laser (pump) was operated at 267 nm, with a bandwidth of 1.2 nm. The FEL pulse (probe) was set at a photon energy of 19.23 eV, corresponding to the fourth harmonic of the seed wavelength of 258 nm. The spectrometer used to collect photoelectrons was a magnetic bottle.[41,42] Electron time-of-flight (TOF) spectra were recorded shot-by-shot while the delay between the pump and probe pulses was scanned with a step of 100 fs. The data used to construct the Fig. 1 consist of 15000 shots per each delay, which were summed and normalized by the summed FEL intensity, recorded simultaneously for every shot. The electron flight times were converted to electron kinetic energies and calibrated according to Ref. 43 with respect to the FEL photon energy. The influence of the FEL and UV intensity on the TOF spectral shape was verified by performing a set of measurements at varied pulse energies and UV focus values. See SI for further details of experimental parameters, sample handling and data analysis.

Computational. In all calculations, CHD and HT were described by extended multi-state complete active space self-consistent field second-order perturbation theory (XMS-CASPT2),[50,51] employing an active space of 6 electrons in 6 orbitals, CAS(6e,6o) (see Fig. S7). In nonadiabatic dynamics simulations, the CASSCF orbitals were averaged over three states with equal weights. The three lowest electronic states of the CHD/HT cation (D_0, D_1, D_2) were taken into account in the computation of the photoelectron spectra. The cc-pVDZ basis set was used in all computations and a real shift of 0.5 Hartree was employed to avoid intruder states in the dynamics. All electronic-structure calculations were performed with the BAGEL program.[52,53]

The photoelectron spectra were computed using the classical limit of the doorway-window formalism.[54,55] Nonadiabatic dynamics simulations were performed with the Tully's fewest switches surface hopping (FSSH) algorithm[56] using an in-house code. The initial conditions were selected from the classical doorway function describing the excitation of the system by the pump pulse in our experiment.

Diabatic states were obtained from the adiabatic states by employing the diabatization scheme of Simah, Hartke, and Werner.[49] To obtain smooth diabatic potentials we included seven states in the calculations (XMS(7)-

CASPT2[6e,6o]). Details of the nonadiabatic dynamics simulations, computation of photoelectron spectra and the diabatization procedure are given in the SI.

ASSOCIATED CONTENT

Supporting Information. Details regarding experimental setup and measurements on FERMI, and the data analysis. Details regarding overall computational methodology, including static multireference calculations, nonadiabatic dynamics, spectrum calculation and diabatization. Results that complement those presented in the manuscript. This material is available free of charge via the Internet at http://pubs.acs.org.

AUTHOR INFORMATION

Corresponding Author

* Nađa Došlić – Ruđer Bošković Institute, Bijenička cesta 54, 10 000 Zagreb, Croatia; Email: nadja.doslic@irb.hr

* Maria Novella Piancastelli – (*i*) Sorbonne Université, CNRS, Laboratoire de Chimie Physique-Matière et Rayonnement, LCPMR, F-75005, Paris, France ; (*ii*) Department of Physics and Astronomy, Uppsala University, SE-751 20 Uppsala, Sweden; Email: maria-novella.piancastelli@physics.uu.se

Author Contributions

M. N. P., R. F., K. C. P. and M. Si. devised the research, O. T., R. J. S., R. R., P. F., M. Di F., A. De F., N. M., M. M., V. Z., T. M., R. G., L. J., C. C., K. C. P., M. Si., R. F., and M. N. P. participated in the conduction of the experimental research, O. T. performed the data analysis, T. P., A. P., M. Sa., P. D., and N. D. devised the theoretical procedure and performed the calculations, M. N. P. and N. D. wrote the paper and all authors discussed the results and commented on the manuscript. Authors‡ O. T. and T. P. contributed equally and are both first authors.

Funding Sources

Croatian Science Foundation (HRZZ IP-2016-06-1142 and IP-2020-02-9932)
Swedish Research Council
Knut and Alice Wallenberg Foundation
COST Action CA18222 (Attosecond Chemistry)

Notes

Any additional relevant notes should be placed here.

ACKNOWLEDGMENT

We are grateful to the FERMI Team and laser group, in particular to L. Giannessi, M. B. Danailov, and A. Demidovich, for their continuous support during the experiments. T. P., A. P., M. Sa, P. D. and N. D thank the Croatian Science Foundation for financial support (IP-2016-06-1142 and IP-2020-02-9932). R. F. thanks the Swedish Research Council and the Knut and Alice Wallenberg Foundation for financial support. We acknowledge the support of the COST Action CA18222 (Attosecond Chemistry). Many fruitful discussions with J. H. D. Eland and W. Domcke are gratefully acknowledged.

ABBREVIATIONS

CHD, 1,3-cyclohexadiene; HT, hexa-1,3,5-triene; CoIn, conical intersection; FEL, free-electron laser; LDM, low-density matter; ESA, excited-state absorption; FC, Franck-Condon; BAC*, extended bond alternating coordinate.

REFERENCES

(1) Deb, S.; Weber, P. M. The ultrafast pathway of photon-induced electrocyclic ring-opening reactions: the case of 1,3-cyclohexadiene. *Annu. Rev. Phys. Chem.* **2011** *62*, 19–39.

(2) Arruda, B. C.; Sension, R. J. Ultrafast polyene dynamics: the ring opening of 1,3-cyclohexadiene derivatives. *Phys. Chem. Chem. Phys.* **2014**, *16*, 4439.

(3) Celani, P.; Olivucci, M.; Bernard, F.; Ottani, S.; Robb, M.A. What happens during the picosecond lifetime of 2A1 cyclohexa-1,3-diene? A CAS-SCF study of the cyclohexadiene/hexatriene photochemical interconversion. *J. Am. Chem. Soc.***1994**, *116*, 10141–10151.

(4) Merchán, M. *et al*. Electronic spectra of 1,4-cyclohexadiene and 1,3-cyclohexadiene: a combined experimental and theoretical investigation. *J. Phys. Chem. A* **1999**, *103*, 5468–5476.

(5) Garavelli, M. *et al*. Reaction path of a sub-200 fs photochemical electrocyclic reaction. *J. Phys. Chem. A* **2001**, *105*, 4458–4469.

(6) Nenov, A. ; Kölle, P. ; Robb, M. A. ; de Vivie-Riedle, R. Beyond the van der Lugt/Oosterhoff model: When the conical intersection seam and the S_1 minimum energy path do not cross. *J. Org. Chem.* **2010**, *75*, 123–129.

(7) Hofmann, A.; de Vivie-Riedle, R. Quantum dynamics of photoexcited cyclohexadiene introducing reactive coordinates. *J. Chem. Phys.* **2000**, *112*, 5054–5059.

(8) Schönborn, J. B.; Sielk, J.; Hartke, B. Photochemical ring-opening of cyclohexadiene: Quantum wavepacket dynamics on a global ab initio potential energy surface. *J. Phys. Chem. A* **2010**, *114*, 4036–4044.

(9) Ohta, A.; Kobayashi, O.; Danielache, S. O.; Nanbu, S. Nonadiabatic ab initio molecular dynamics of photoisomerization reaction between 1,3-cyclohexadiene and 1,3,5-cis-hexatriene. *Chem. Phys.* **2015**, *459*, 45–53.

(10) Lei, Y.; Wu, H.; Zheng, X.; Zhai, G.; Zhu, C. Photo-induced 1,3-cyclohexadiene ring opening reaction: Ab initio on-the-fly nonadiabatic molecular dynamics simulation. *J. Photochem. Photobiol. A Chem.* **2016**, *317*, 39–49.

(11) Schalk, O. *et al*. Cyclohexadiene revisited: A time-resolved photoelectron spectroscopy and ab initio study. *J. Phys. Chem. A* **2016**, *120*, 2320–2329.

(12) Polyak, I.; Hutton, L.; Crespo-Otero, R.; Barbatti, M.; Knowles, P. J. Ultrafast photoinduced dynamics of 1,3-cyclohexadiene using XMS-CASPT2 surface hopping. *J. Chem. Theory Comput.* **2019**, *15*, 3929–3940.

(13) Kotur, M.; Weinacht, T.; Pearson, B. J.; Matsika, S. Closed-loop learning control of isomerization using shaped ultrafast laser pulses in the deep ultraviolet. *J. Chem. Phys.* **2009**, *130*, 134311.

(14) Attar, A. R. *et al*. Femtosecond x-ray spectroscopy of an electrocyclic ring-opening reaction. *Science* **2017**, *356*, 54–59.

(15) Adachi, S.; Sato, M.; Suzuki, T. Direct observation of ground-state product formation in a 1,3-cyclohexadiene ring-opening reaction. *J. Phys. Chem. Lett.* **2015**, *6*, 343–346.

(16) Pemberton, C. C.; Zhang, Y.; Saita, K.; Kirrander, A.; Weber, P. M. From the (1B) spectroscopic state to the photochemical product of the ultrafast ring-opening of 1,3-cyclohexadiene: A

spectral observation of the complete reaction path. *J. Phys. Chem. A* **2015**, *119*, 8832–8845.

(17) Petrović, V. S. *et al*. Transient X-ray fragmentation: probing a prototypical photoinduced ring opening. *Phys. Rev. Lett.* **2012**, *108*, 253006.

(18) Wolf, T. J. A. *et al*. The photochemical ring-opening of 1,3-cyclohexadiene imaged by ultrafast electron diffraction. *Nat. Chem.* **2019**, *11*, 504–509.

(19) Karashima, S. *et al*. Ultrafast ring-opening reaction of 1,3-cyclohexadiene: identification of nonadiabatic pathway via doubly excited state. *J. Am. Chem. Soc.* **2021**, *143*, 8034–8045.

(20) Minitti, M. P. *et al.* Imaging Molecular Motion: Femtosecond X-Ray Scattering of an Electrocyclic Chemical Reaction. *Phys. Rev. Lett.* **2015**, *114*, 255501.

(21) Kosma, K; Trushin, S. A.; Fuß, W. & Schmid, W. E. Cyclohexadiene ring opening observed with 13 fs resolution: coherent oscillations confirm the reaction path. *Phys. Chem. Chem. Phys.* **2009**, *11*, 172–181.

(22) Havinga, E.; Schlatmann, J. L. M. A. Remarks on the specificities of the photochemical and thermal transformations in the vitamin D field. *Tetrahedron* **1961**, *16*, 146–152.

(23) Anderson, N. A.; Shiang, J. J.; Sension, R. J. Subpicosecond ring opening of 7-dehydrocholesterol studied by ultrafast spectroscopy. *J. Phys. Chem. A* **1999**, *103*, 10730–10736.

(24) Matsuda, K.; Irie, M. Diarylethene as a photoswitching unit. *J. Photochem. Photobiol. C Photochem. Rev.* **2004**, *5*, 169–182.

(25) Kobatake, S.; Takami, S.; Muto, H.; Ishikawa, T.; Irie, M. Rapid and reversible shape changes of molecular crystals on photoirradiation. *Nature* **2007**, *446*, 778–781.

(26) Irie, M.; Fukaminato, T.; Matsuda, K.; Kobatake, S. Photochromism of diarylethene molecules and crystals: memories, switches, and actuators. *Chem. Rev.* **2014**, *114*, 12174–12277.

(27) Dattler, D. *et al*. Design of collective motions from synthetic molecular switches, rotors, and motors. *Chem. Rev.* **2020**, *120*, 310–433.

(28) Baroncini, M.; Silvi, S.; Credi, A. Photo- and redox-driven artificial molecular motors. *Chem. Rev.* **2020**, *120*, 200–268.

(29) Woodward, R. B.; Hoffmann, R. The conservation of orbital symmetry. *Angew. Chemie Int. Ed.* **1969**, *8*, 781–853.

(30) Van der Lugt, W. T. A. M.; Oosterhoff, L. J. Quantum-chemical interpretation of photo-induced electrocyclic reactions. *Chem. Commun.* **1968**, 1235–1236.

(31) Van der Lugt, W. T. A. M.; Oosterhoff, L. J. Symmetry control and photoinduced reactions. *J. Am. Chem. Soc.* **1969**, *91*, 6042–6049.

(32) Pariser, R. Theory of the electronic spectra and structure of the polyacenes and of alternant hydrocarbons. *J. Chem. Phys.* **1956**, *24*, 250–268.

(33) Nakayama, K.; Nakano, H.; Hirao, K. Theoretical study of the π→π* excited states of linear polyenes: The energy gap between $1^1B_u^+$ and $2^1A_g^-$ states and their character. *Int. J. Quantum Chem.* **1998**, *66*, 157–175.

(34) Domcke, W.; Yarkony, D. R.; Köppel, H. *Conical Intersections: Theory, Computation and Experiment*; World Scientific, Singapore, 2011.

(35) Nakamura, H. *Nonadiabatic Transition: Concepts, Basic Theories and Applications*; World Scientific, Singapore, 2012.

(36) Yarkony, D. R. Nonadiabatic quantum chemistry—past, present, and future. *Chem. Rev.* **2012**, *112*, 481–498.

(37) Domcke, W.; Stock, G. Theory of ultrafast nonadiabatic excited-state processes and their spectroscopic detection in real time, *Adv. Chem. Phys.* **1997**, *100*, 1-169.

(38) Squibb, R.J. *et al*. Acetylacetone photodynamics at a seeded free electron laser. *Nat. Commun.* **2018**, *9*, 63.

(39) Pathak, S. *et al*. Tracking the ultraviolet-induced photochemistry of thiophenone during and after ultrafast ring opening. *Nat. Chem.* **2020**, *12*, 795–800.

(40) Svetina, C. *et al*. The low density matter (LDM) beamline at FERMI: optical layout and first commissioning. *J. Synchrotron Radiat.* **2015**, *22*, 538–543.

(41) Eland, J. H. D. *et al*. Complete two-electron spectra in double photoionization: the rare gases Ar, Kr, and Xe. *Phys. Rev. Lett.* **2003**, *90*, 053003.

(42) Eland, J. H. D.; Linusson, P.; Mucke, M.; Feifel, R. Homonuclear site-specific photochemistry by an ion–electron multicoincidence spectroscopy technique. *Chem. Phys. Lett.* **2012**, *548*, 90–94.

(43) Kimura, K. *et al*., *Handbook of HeI Photoelectron Spectra of Fundamental Organic Molecules*; Japan Scientific Societies Press, Tokyo, 1981; p. 68.

(44) Beez, M.; Bieri, G.; Bock, H.; Heilbronner, E. *Helvetica Chim. Acta* **1973**, *56*, 1028-1046.

(45) Robin, M. B. *Higher Excited States of Polyatomic Molecules* Vol. 2; Academic Press, New York, 1975.

(46) McDiarmid, R.; Sabljić, A.; Doering, J. P. Valence transitions in 1,3-cyclopentadiene, 1,3-cyclohexadiene, and 1,3-cycloheptadiene. *J. Chem. Phys.* **1985**, *83*, 2147–2152.

(47) Ning, J.; Truhlar, D. G. The valence and Rydberg states of dienes. *Phys. Chem. Chem. Phys.* **2020**, *22*, 6176–6183.

[48] McDiarmid, R.; Sabljić, A.; Doering, J. P. Valence transitions in 1,3-cyclopentadiene, 1,3-cyclohexadiene, and 1,3-cycloheptadiene. *J. Chem. Phys*. **1985**, *83*, 2147–2152.

(49) Simah, D.; Hartke, B.; Werner, H.-J. Photodissociation dynamics of H2S on new coupled ab initio potential energy surfaces. *J. Chem. Phys.* **1999**, *111*, 4523–4534.

(50) Shiozaki, T.; Győrffy, W.; Celani, P.; Werner, H.-J. Communication: Extended multi-state complete active space second-order perturbation theory: Energy and nuclear gradients. *J. Chem. Phys.* **2011**, *135*, 081106.

(51) Park, J. W.; Shiozaki, T. On-the-fly CASPT2 surface-hopping dynamics. *J. Chem. Theory Comput.* **2017**, *13*, 3676–3683.

(52) Shiozaki, T. BAGEL: Brilliantly advanced general electronicstructure library. *Wiley Interdiscip. Rev.: Comput. Mol. Sci.* **2018**, *8*, el1311.

(53) Shiozaki, T. BAGEL: Brilliantly Advanced General Electronic-structure Library. http://www.nubakery.org under the GNU General Public License.

(54) Gelin, M.F. *et al*. Ab initio surface-hopping simulation of femtosecond transient-absorption pump–probe signals of nonadiabatic excited-state dynamics using the doorway–window representation. *J. Chem. Theory Comput.* **2021**, *17*, 2394–2408.

(55) Piteša, T. *et al*. Combined Surface-Hopping, Dyson Orbital, and B-Spline Approach for the Computation of Time-Resolved Photoelectron Spectroscopy Signals: The Internal Conversion in Pyrazine. *J. Chem. Theory Comput.* **2021**, *17*, 5098–5109.

(56) Tully, J. Molecular dynamics with electronic transitions. *J. Chem. Phys.* **1990**, *93*, 1061.

SYNOPSIS TOC (Word Style "SN_Synopsis_TOC"). If you are submitting your paper to a journal that requires a synopsis graphic and/or synopsis paragraph, see the Instructions for Authors on the journal's homepage for a description of what needs to be provided and for the size requirements of the artwork.

To format double-column figures, schemes, charts, and tables, use the following instructions:

Place the insertion point where you want to change the number of columns
From the **Insert** menu, choose **Break**
Under **Sections**, choose **Continuous**
Make sure the insertion point is in the new section. From the **Format** menu, choose **Columns**
In the **Number of Columns** box, type **1**
Choose the **OK** button

Now your page is set up so that figures, schemes, charts, and tables can span two columns. These must appear at the top of the page. Be sure to add another section break after the table and change it back to two columns with a spacing of 0.33 in.

Table 1. Example of a Double-Column Table

Column 1	Column 2	Column 3	Column 4	Column 5	Column 6	Column 7	Column 8

Authors are required to submit a graphic entry for the Table of Contents (TOC) that, in conjunction with the manuscript title, should give the reader a representative idea of one of the following: A key structure, reaction, equation, concept, or theorem, etc., that is discussed in the manuscript. Consult the journal's Instructions for Authors for TOC graphic specifications.

Insert Table of Contents artwork here